ARTICLE

Determining the sequence and backbone structure of "semi-statistical" copolymers as donor-acceptor polymers in organic solar cells

Received 00th January 20xx,
Accepted 00th January 20xx

DOI: 10.1039/x0xx00000x

Samuel S. Lawton[a], Daniel Warr[a], Luís M. A. Perdigão[a], Yujing Chang[a], Agnieszka Pron[b], Giovanni Costantini[a], David M. Haddleton*[a]

Organic photovoltaics (OPVs) are attracting significant attention due to the growing demand for economically viable and renewable energy sources. With efficiencies exceeding 16.5 %, single junction bulk heterojunction (BHJ) devices are amongst the most promising and are nearing commercialisation. One recent avenue of research has focused on statistical conjugated copolymers. However, a detailed investigation as to why these materials can achieve higher power conversion efficiencies than their regular alternating counterparts is seldom reported. This work describes an investigation into donor-acceptor polymers demonstrating how differing monomer activities can lead to differing microstructures in a simple batch reaction, which in turn demonstrate promising optoelectronic and morphological properties required for organic photovoltaic devices. A one pot condensation polymerisation reaction with three monomers leads to an ABA triblock structure from differing monomer reactivity's. This structure in turn leads to visualised phase separation which is possibly linked to an increase in performance. Further to this we report on the reliability of the Stille coupling for the synthesis of conjugated polymers.

Introduction

Organic photovoltaics (OPVs) based on bulk heterojunction (BHJ) devices is becoming an increasingly viable alternative to silicon solar cells, with efficiencies now exceeding 16.5 % for single junction devices.[1] Efficiencies are improved by the use of non-fullerene small-molecule acceptors incorporated as a d component in binary blends. Despite efficiencies being lower than that of current silicon based devices, OPVs are often more cost effective with energy payback times reduced to days[2], compared to years for silicon devices.[3] OPVs offer further benefits such as their low production costs, light weight and the ability to be flexible and semi-transparent[4, 5] making them particularly appealing for a direct integration in modern architecture, as demonstrated by BELECTRIC and Merck with the solar tree instalment at the Universal Exhibition in Milan, this current work has been designed to carry out a systematic study on why these particular materials are effective.[6]

A widely investigated area of OPVs has been the use of polymer-donor, fullerene-acceptor BHJs. Typically, such devices are formed through a physical blend of an electron donating polymer and an electron accepting fullerene. Phenyl-C_{61}-butyric acid methyl ester ($PC_{61}BM$) is used as a cost effective electron accepting material, although often the more expensive $PC_{71}BM$ is chosen as an alternative, owing to its improved solar absorption spectrum.

A contributing factor to the increase in the power conversion efficiency (PCE) of polymer/fullerene BHJ devices can largely be accredited to the development of so called push-pull, or donor-acceptor, polymers which facilitate the tuning of the materials electronic properties.[7-10] Donor-acceptor polymers typically consist of a conjugated backbone comprised of alternating electron rich (donor) and electron poor (acceptor) moieties.[11] The energy levels of the donor polymer can be tuned through selection of both the donor and acceptor.[7, 12-15] More recently "statistical" and "semi-statistical" terpolymers have gained increasing attention in the field.[16-19]

While alternating donor-acceptor polymers have regular monomer sequences, statistical copolymers have a less well-defined distribution of monomers. Coupled with variations in conjugation length along the backbone, this non-regular distribution of different sequences can give rise to diverse chromophores in statistical and semi-statistical copolymers. This often leads to changes in the spectral absorption and adjustments in the HOMO which, in-turn, influence the short circuit current (J_{sc}) and open circuit

[a] Department of Chemistry, University of Warwick, Coventry, CV4 7AL, UK.
[b] Merck Chemicals Ltd. University Pkwy, Chilworth, Southampton SO16 7QD
Electronic Supplementary Information (ESI) available. See DOI: 10.1039/x0xx00000x

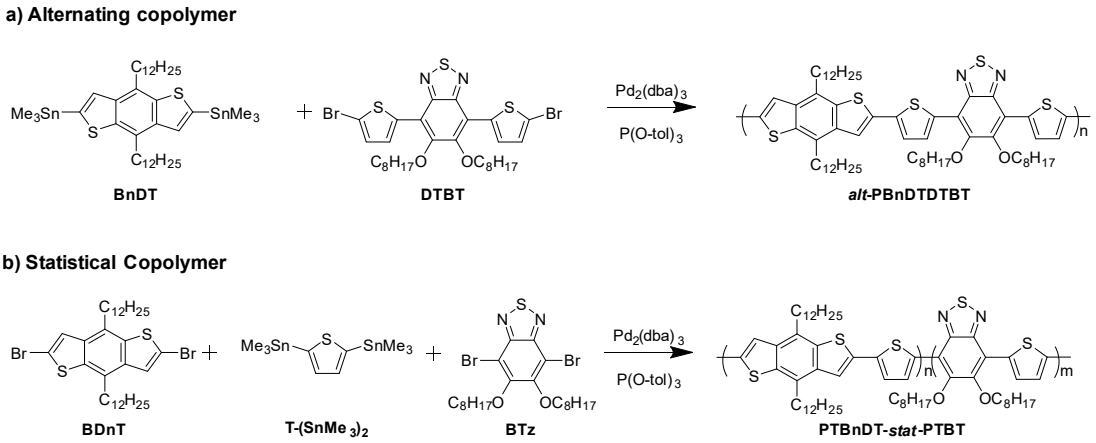

Figure 1. Reaction scheme for the formation of a; *alt*-PBnDTDTBT and b; PTBnDT-*stat*-PTBT formed in this work.

voltage (V_{oc}), respectively.[20-23] The nanocrystalline morphologies sometimes found in statistical copolymers have been shown to hinder charge extraction and decrease J_{sc}.[24,22, 25] The tendency of statistical copolymers to aggregate less than their alternating counterparts can, however, be advantageous, leading to materials which are more readily soluble and easier to process.[26] There is a significant amount of trial and error in determining whether a statistical or semi-statistical copolymer will outperform its alternating counterpart. Indeed, both statistical and regular alternating copolymers have been reported to outperform their counterparts and it is not possible to predict which polymer structure is best.[23, 26, 27]

In polymers monomer sequence is often the key to achieving targeted properties. Despite this being true also for conjugated polymers the effect of the precise backbone sequence is only seldom analysed. One study by Meyer and co-workers investigated a range of benzothiadiazol-phenylvinylene oligomers and concluded that sequence had a profound influence on both optoelectronic properties and solid state packing.[28] A second study investigated how the properties of PTB7-Th vary when synthesised using different catalysts with a significant difference in monomer ratios within the polymer backbone observed leading to enhanced pre-aggregation in solution and markedly different photovoltaic properties.[29] Molecular weight and dispersity have been shown to have significant effects on the morphology and electronic properties of conjugated polymers films[30-33] and, as such, the direct comparison of the properties of these two polymers is problematic. Sommer and co-workers identified homocouplings as critical side reactions in direct arylation polycondensation and quantified them by using size exclusion chromatography (SEC) and NMR spectroscopy.[34] Evidence of the high level of infidelity in the Stille coupling was also recently presented by Warr *et al.* who imaged defects caused by the homo-coupling of furan rings in poly(tetradecyl-diketopyrrolopyrrole-furan-*co*-furan) by high resolution scanning tunnelling microscopy (STM).[35]

The PTBnDT-*stat*-PTBT polymer backbone studied in this current work is comprised of a statistical distribution of benzothiadiazole (BT) accepting units and benzodithiophene (BDT) donating units, each separated by a thiophene bridge. The BT acceptor retains its aromatic stabilisation in the quinodal form, helping to stabilise the LUMO of the polymer. Compared to the benzotriazole (BTz) analogue, BT has been shown to produce materials with a much lower E_g and improved J_{sc}.[36,37, 34, 3534-35] BnDT has been a popular choice as an electron donating

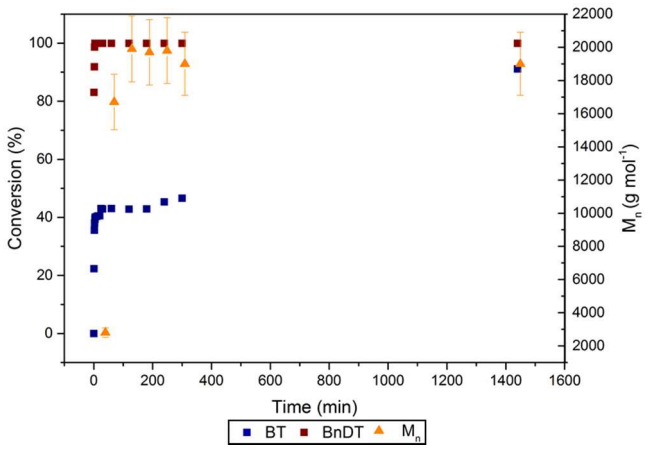

Figure 3 Monomer conversion of BnDT (red) and BT (blue) during a Stille polycondensation, using $Pd_2(dba)_3$ (2.5 mol %) and $P(o\text{-tolyl})_3$ (7.5 mol %) as the catalyst . Number average molecular weight (M_n) is shown in orange.

(push) species since it was introduced in 2008 by Hou *et al.*,[38] as its fused aromatic structure favours a greater degree of π-π stacking leading to more crystalline morphologies and enhancing hole mobilities.[14, 36] The thiophene bridge acts as a spacer between two adjacent units lowering the torsional strain caused by the solubilising side chains and can also act as a secondary acceptor for BT.[40] It is noted that in recent work from Voit it has been shown that when AB type monomers are used as opposed to AA and BB can result in higher synthetic efficiencies. [37]In previous work, Merck have demonstrated that the statistical copolymer PBTT-*stat*-PBDTT (from an AA and two BB type monomers) outperforms the corresponding regularly alternating copolymer PDTBTBDT.[6] This work set out to investigate possible reasons behind this. Herein, we investigate the structural differences that give rise to the higher J_{sc}, V_{oc} and FF. The work was designed to investigate the reasons why some copolymers formed from the same monomers performed better than others when the only apparent difference was the method of synthesis and order of monomer addition. We chose to look at each monomer conversion to see relative rates of consumption. The sequence distribution was visualised by high resolution STM which allowed us to see how each monomer was incorporated into the copolymer. We demonstrate that the two AA dibrominated monomers of distinctly different electronic properties proceed through the Stille catalytic cycle at very different rates giving rise to a relatively ordered ABA block copolymer rather than to a statistical arrangement of the donor and acceptor units along the backbone. This is presented as a reason for the differences in performance relating OPV performance to molecular structure for the first time.

Results and discussion

Whilst ^{1}H and ^{13}C NMR analysis of the final product is a powerful tool for characterisation, it becomes increasingly complex as regularity decreases in the polymeric chains. As such, analysing the NMR spectra for both the alternating and the statistical copolymers, Figure 1, does not provide significant structural information. Conversely, in this instance monomer conversion can be followed by ^{1}H NMR with relative ease. When BnDT and BT are converted to the polymer, a shift in the signal at 3.15 and 4.35 ppm (respectively) is observed. These signals correspond to the α-CH_2 groups of the side chains on each monomer. Covalent coupling to the thiophene and an increase in conjugation in the system leads to a significant change in the observed chemical shift of the α-CH_2 (Figure S1).

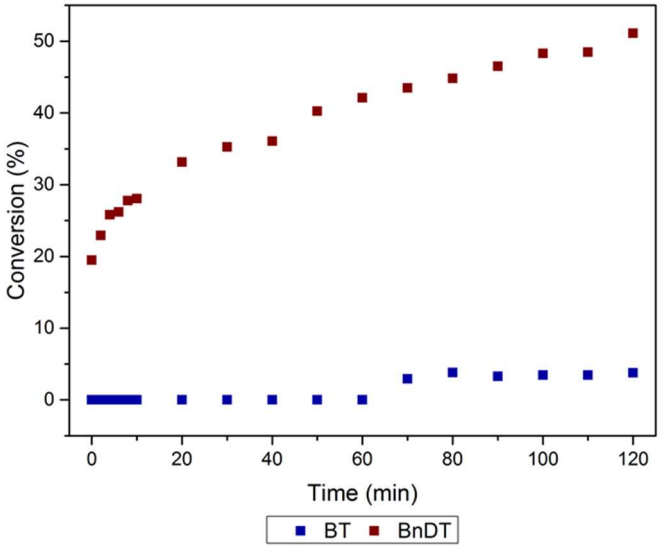

Figure 2 Conversion of BnDT and BT with tri($SnBu_3$) measured by in-situ ^{1}H NMR.

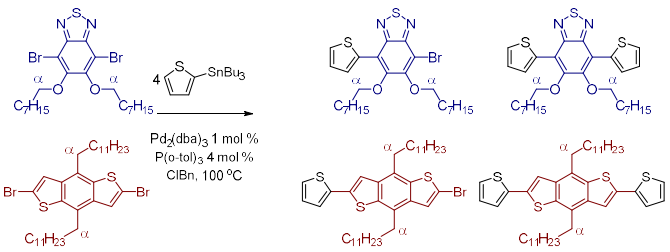

Scheme 1 Competitive reaction between BT (blue) and BnDT (red) with 2-tributylstannyl thiophene under an argon atmosphere, performed in an NMR tube fitted with a Young's tap and analysed in-situ.

For the initial investigation of the conversion of BnDT and BT in this Stille polycondensation, we replaced the di-functional bis-2,5-(trimethylstannyl) thiophene with the mono-functional 2-tri-butylstannyl thiophene (Scheme 1). The mono-functional thiophene limits the number of possible products to just four, thus making ^{1}H NMR interpretation easier. The reaction was carried out on a small scale in an NMR tube fitted with a Young's tap, under a blanket of argon with which *in-situ* ^{1}H NMR spectra could be recorded up to every two minutes.

The triplet from the BnDT monomer was observed at δ = 3.15 ppm; as the reaction progresses the intensity of this peak is reduced and the emergence of two new triplets is observed, at δ = 3.30 ppm and at δ = 3.45 ppm, assigned to the mono (TBnDT) and di-substituted (DTBnDT) BnDT monomer, respectively. The BT monomer behaves in a similar manner shifting from δ = 4.35 to δ = 4.45 ppm, albeit to a much lesser extent. At t = 120 min a low intensity peak at δ = 4.45 ppm can be observed which is assigned to the mono-substituted BT unit (TBT), while there is no visible peak for the di-substituted species (DTBT) observed within this reaction time frame. The consumption of BT and BnDT is plotted against time in Figure 2 and shows an initial (t = 0 to t = 10 min) rapid conversion of BnDT followed by a steady rate of consumption. BT shows no conversion (within the noise limit/error of NMR (5 %)) until much later at t = 70 min.

In-situ ^{1}H NMR studies offer a good insight into how each monomer is consumed in the Stille reaction with some limitations. These include the small scale of the reaction, temperature limitations on the NMR equipment and the inability for mechanical stirring. While microwave synthesis is largely reported in the literature as a standard synthetic

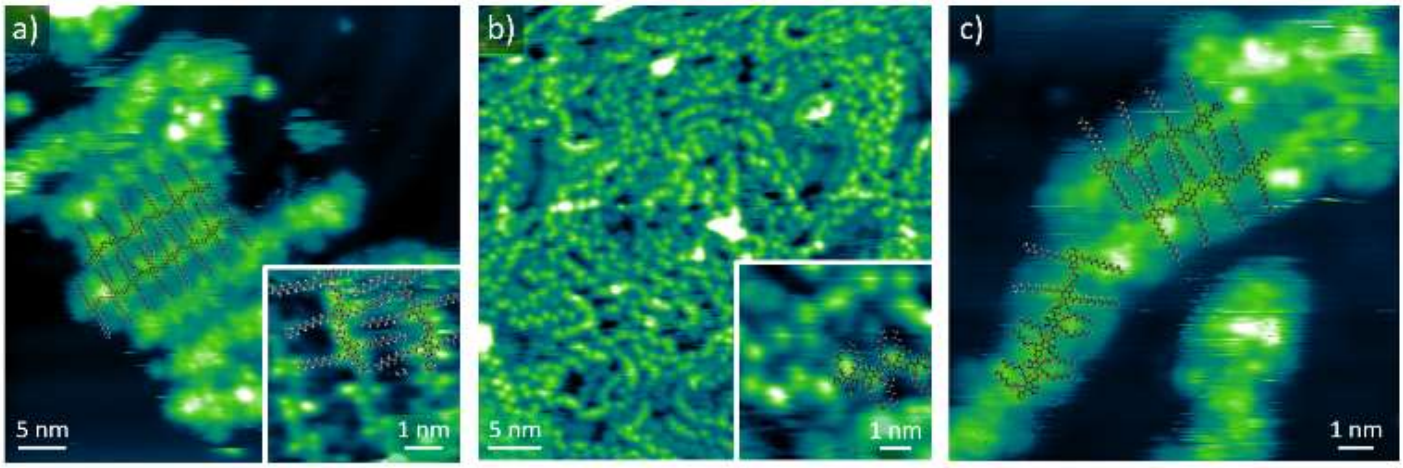

Figure 4 STM images of the polymers deposited by ESD on a Au(111)/mica surface. (a) PTBnDT homopolymers, inset showing a magnified view of a different region. Main image: V_{bias} = −3.0 V, I = 100 pA; inset: V_{bias} = −1.5 V, I = 50 pA. (b) PTBT homopolymers, inset showing a magnified view of the same region. V_{bias} = −2.0 V, I = 100 pA. (c) PTBnDT-stat-PTBT copolymer. V_{bias} = −2.5 V, I = 100 pA. Scaled molecular models of the corresponding polymers are superimposed on the images.

procedure,[38, 39] we elected to use conventional heating as it could mirror industrial scale up. Although conventional heating leads to a slower reaction rate than microwave synthesis, it has greater industrial appeal due to its scalability and compatibility with well-established industrial reactor designs, as well as allowing for ease of sampling throughout the reaction unlike microwave synthesis.

In order to investigate the effect of different monomer reactivities a reaction mixture containing 1.0 mmol of 2,5-bis(trimethylstannyl) thiophene, 0.5 mmol of BnDT and 0.5 mmol of BT in 48 ml of chlorobenzene was heated to 133 °C. 2.0 ml of catalyst solution containing 0.020 mmol $Pd_2(dba)_3$ and 0.120 mmol P(*o*-tolyl)$_3$ were added and the reaction was sampled over time. Owing to the large number of molecular species formed, the resolution of individual products is more difficult in the case of polymerisation, but it is still possible to observe the consumption of monomers with ^{1}H NMR by measuring the depletion of the monomer peak against all other species α-CH_2 signals (figure S19). In agreement with the *in-situ* studies, the BnDT monomer is depleted more rapidly than the BT monomer (Figure 3). An overall more rapid conversion of both the BnDT and BT monomer is observed resulting from the faster reacting 2,5-bis(trimethylstannyl) thiophene. The BnDT monomer is converted from its unsubstituted form rapidly within the first 10 minutes. Interestingly, unlike the *in-situ* reaction, discussed above, the BT monomer shows initial rapid conversion, before slowing at approximately 30 minutes, when the 2,5-bis(trimethylstannyl) thiophene monomer is mostly consumed and the reaction slows accordingly.

Molecular weights (M_n >15 kDa by gel permeation chromatography, GPC) are reached at relatively low monomer conversion. The polymers formed in the first 200 minutes of the reaction are enriched in BnDT and as time progresses more BT is incorporated into the polymer. Interestingly the number average molecular weight profile of the polymerisation (Figure 3) is what one would expect from a chain growth. From the evidence presented we determined that the materials being produced are gradient- or block-like copolymers in character.

Further evidence of the block-like structure resulting from the statistical copolymerisation is provided by ultrahigh vacuum STM imaging of the polymers deposited on a Au(111)/mica surface by vacuum electrospray deposition (ESD).[35] Figure 4 shows the comparison between the STM images of the PTBnDT (Figure 4a), the PTBT (Figure 4b), and the PTBnDT-*stat*-PTBT copolymer (Figure 4c). Individual PTBnDT strands can be clearly recognised in Figure 4a, with the backbones appearing brighter than the alkyl side chains. Their measured periodicity fits well with the value predicted by molecular modelling (1.22 nm from the MMFF94s force field in the Avogadro molecular editor) and a scaled molecular model is in excellent agreement with the details of the STM images (inset of Figure 4a). In particular, the backbone shows a small undulation characteristic of an all-trans conformation of the TBnDT units, and two brighter lobes can be seen on both sides of each TBnDT, which are probably due to the slightly higher position of the first sp^3 carbon in the alkyl chains. The backbones of neighbouring molecules lie parallel to each other and the side chains interdigitate to maximise van der Waals contact, giving rise to small, locally highly ordered molecular islands.

PTBT homopolymers appear much less ordered and display a higher degree of curvature in the STM images (Figure 4b), denoting a higher flexibility that is expected from their molecular structure. Locally straight segments composed of pairs of bright lobes positioned on alternating sides of the main molecular axis have a periodicity close to that estimated by molecular modelling for PTBT (around 0.83 nm). A scaled molecular model with the BT units all trans to each other fits well with the STM images (inset of Figure 4b), demonstrating that the bright lobes correspond to the initial, highly non-planar sections of the side chains.

Finally, Figure 4c shows a STM image obtained by depositing the PTBnDT-*stat*-PTBT copolymer (with a nominal 1:1 ratio of

TBnDT to TBT). By comparison with the images of the homopolymers (Figures 4a and 4b), it is easy to recognise that the copolymer is constituted by sections where several TBnDT units are followed by several TBT units, i.e. that its sequence is randomly block-like. Homo-PTBnDT strands were also observed in the same sample (images not shown), which is a further indication that this is not an ordered alternating copolymer. We cannot exclude that the different solubilities of the different types of sequences might influence the distribution of the molecules that are deposited on the surface[43] and thus imaged by STM. However, in conjunction with the kinetic studies presented earlier, the ESD-STM results

Table 1 Summary of ligand oxidation on-sets and cone angles.

Ligand	Onset to Oxidation (V (vs. Ag/AgCl)	Cone angle (°)	Chemical shift (ppm)
Tris-(2,4,6-trimethylphenyl)phosphine)	0.92	212[40]	-36.50
XPhos	1.12	210[40]	-12.37
Tris(2,4-dimethylphenyl)phosphine	1.22	150-210	-32.03
Tris(2-methoxyphenyl)phosphine	1.27	137[40]	-39.24
Tris(*o*-tolyl)phosphine	1.31	147[40]	-29.62
Triphenyl phosphite	1.55	140-160[41]	-17.55

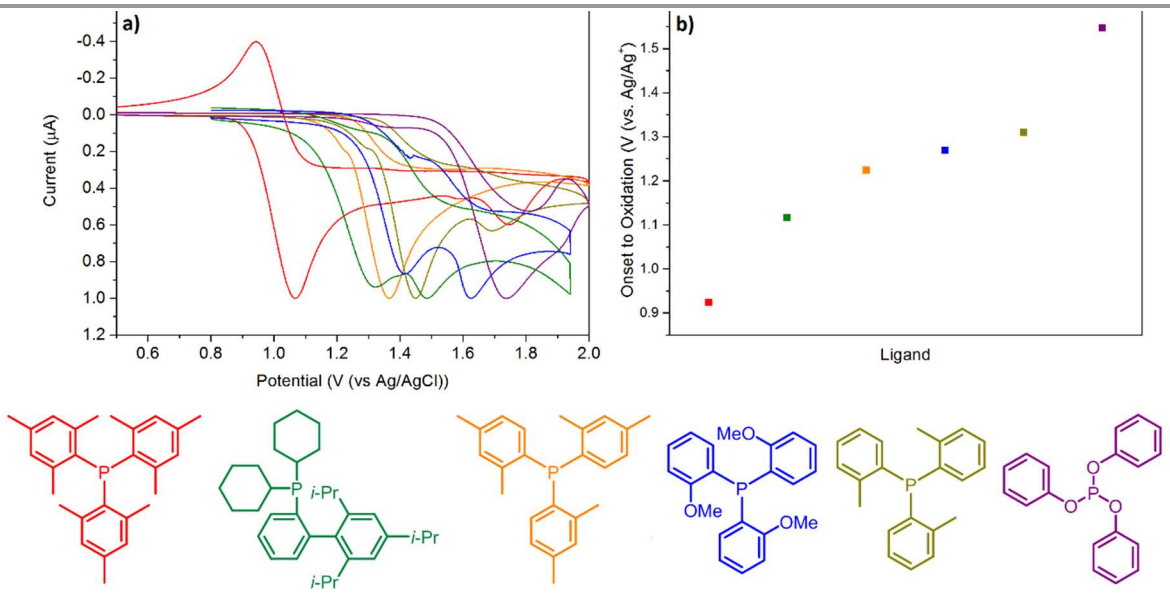

Figure 5 Summary of electronic properties of ligands; left CV of 10 μM solutions of ligand, right, onset of oxidation of ligand solution.

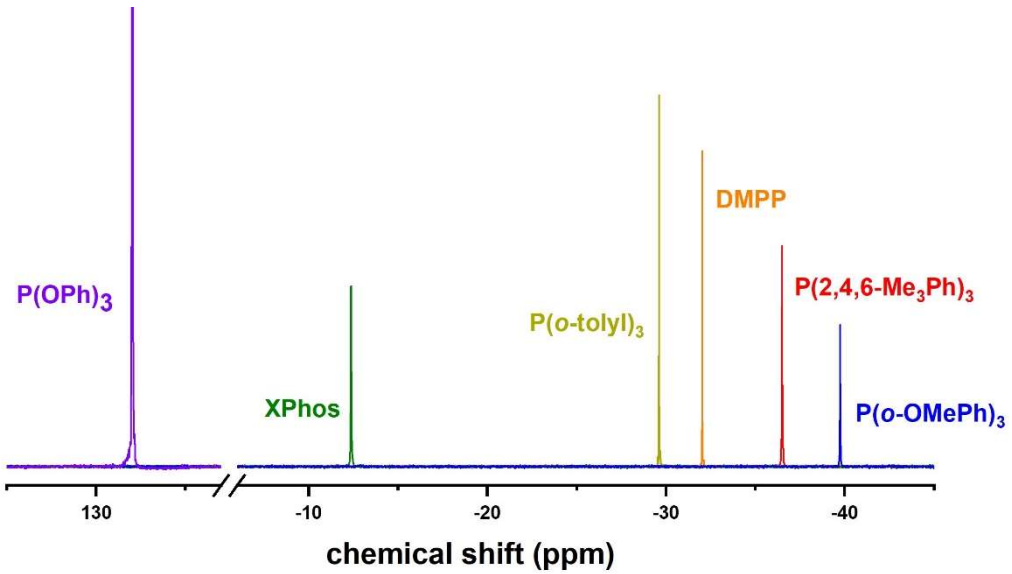

Figure 6 ^{31}P-NMR spectra of ligands (in CDCl3).

further support the block-like structure of the PTBnDT-*stat*-PTBT copolymer. We note that the images in figure 4 are not necessarily representative of the bulk sample.

We hypothesise that the greater rate of conversion of the BnDT unit (which gives rise to the polymers block-like structure) can be attributed to the lower steric demand around the C-Br

Table 2 Summary of properties of polymers resulting from the use of different ligands. M_n, M_w and Đ determined by high temperature GPC. Td is defined as 5 % mass loss determined by thermal gravimetric analysis.

Polymer	Yield (%)	M_n (g/mol)	M_w (g/mol)	Đ	% BnDT (NMR)	% BT (NMR)	T_D (°C)
XPhos	90.8	20700	53900	2.42	47	53	330
DMPP	76.9	18100	33400	1.85	57	43	329
P(*o*-OMePh)$_3$	84.2	18200	35800	1.97	52	48	333
P(*o*-tolyl)$_3$	81.6	17600	44800	2.55	50	50	329

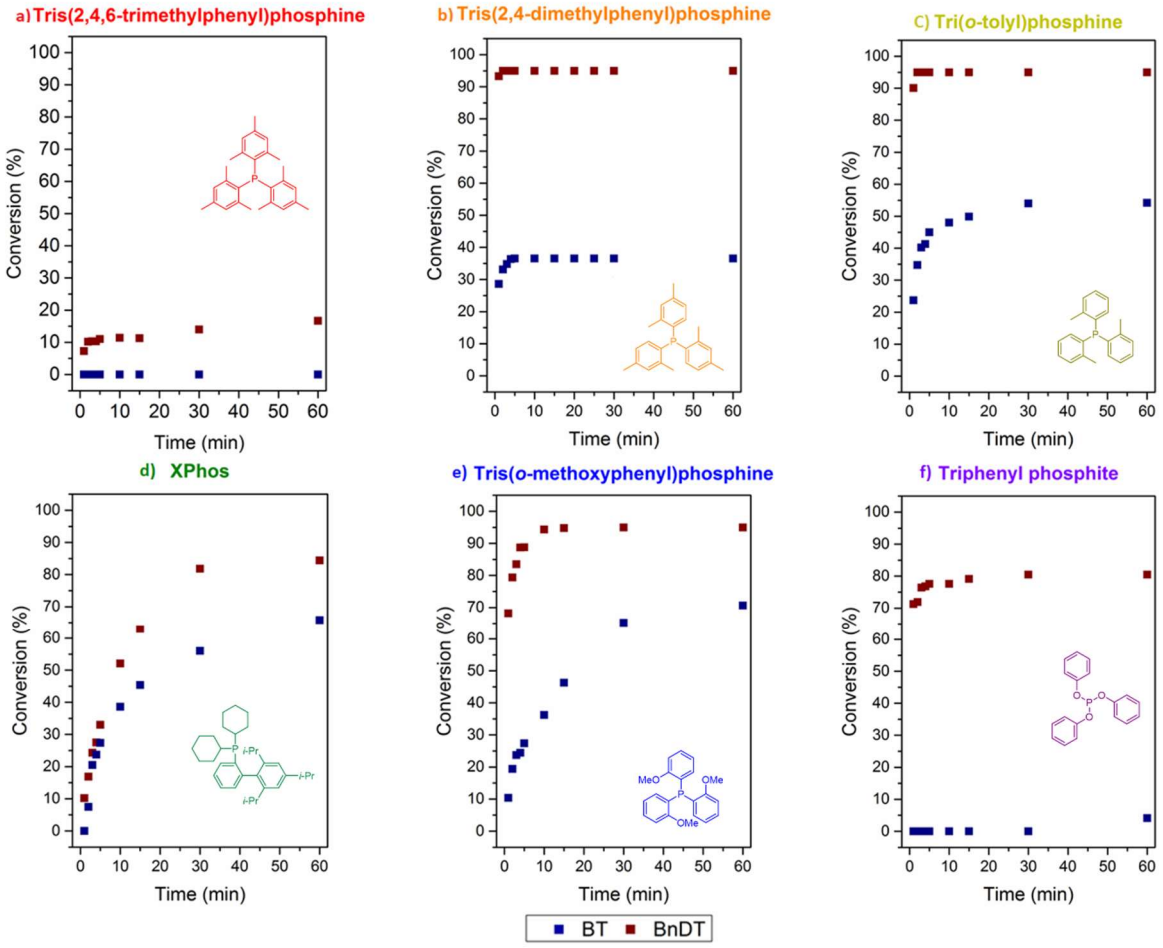

Figure 7 Conversion of BnDT and BT in the first 60 minutes of Stille polycondensation with differing ligands, depicted within.

bond in BnDT *vs* that of BT, as well as to the greater stability of the Pd complex formed on oxidative addition of the monomer to the electron deficient palladium. In order to further investigate the effect of the catalyst on the formation of the polymers and their related properties, we varied the P-ligands on the palladium catalyst. Ligands were selected to have a variety of electron donor abilities as well as varying steric bulk. In particular, ligands with additional electron donating groups on the phenyl rings – including methyl and methoxy substituents – were used and their donor ability was screened qualitatively by cyclic voltammetry (CV), Figure 5. Further to the more electron rich triphenyl phosphine derivatives we also examined the use of the popular Buchwald ligand XPhos which is frequently used in the palladium catalysed cross-coupling reactions.[42, 43] Moreover, we also employed a more electron withdrawing ligand, triphenyl phosphite (P(OPh)$_3$). The steric impact of each of these ligands is considered by the literature values for their cone angles, Table 1.

The values for the onset for oxidation of the ligands (Figure 5b) follow an expected trend, with the most difficult to oxidise being triphenyl phosphite, as the electron withdrawing oxygen atoms adjacent to the phosphine result in a more tightly bound

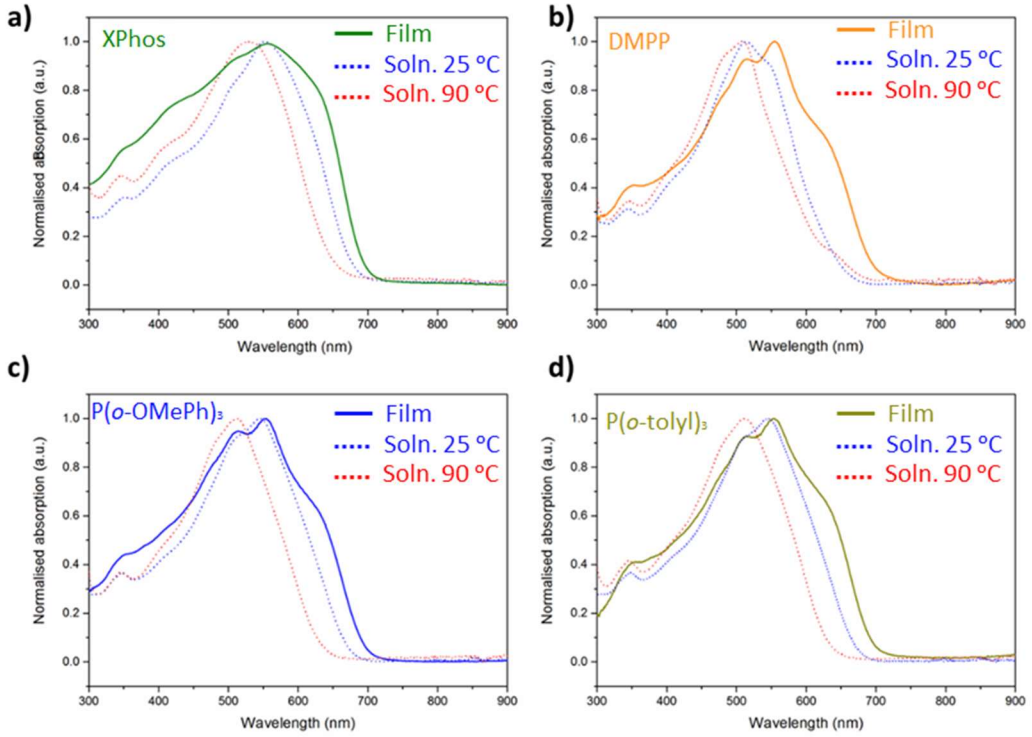

Figure 8 UV-Vis spectra of four polymers synthesised with use of different ligands in the Stille coupling.

lone pair and thus a greater potential is required to remove an electron. Tris(*o*-tolyl)phosphine (P(*o*-tolyl)$_3$) oxidises with relative ease compared to the P(OPh)$_3$ species owing to the reduced electron withdrawing ability of the phenyl rings, although the phosphorous lone pair is involved in conjugation with the aromatic rings. The *ortho*-methoxy group in tris(2-methoxyphenyl)phosphine (P(*o*-OMePh)$_3$) pushes more electron density into the aromatic system, resulting in the lone pair of the phosphine being involved in conjugation with the phenyl rings to a lesser extent (than P(*o*-tolyl)$_3$). For tris-(2,4-dimethylphenyl) phosphine (DMPP) the two methyl groups increase the electron density of the ring and therefore the ease of oxidation from the phosphorus *via* lone pair (there is no literature value for the cone angle of this rarely used ligand). The most readily oxidised ligand P(2,4,6-Me$_3$Ph)$_3$ also has the largest cone angle of 212°. The methyl groups which are in close proximity result in rotation of the aromatic systems to minimise steric interactions thus accounting for the high cone angle. Not only do the methyl groups have a large steric effect but their electron donation into the phenyl rings results in a greatly reduced participation of the phosphorous lone pair in conjugation, with the aromatic system causing the lowest oxidation potential observed of 0.92 V.

Phosphorous NMR (^{31}P-NMR) was also used to probe the electronic properties of these ligands, Figure 6 and Table 1. It could be found that the electron-donating abilities of P(OPh)$_3$, P(*o*-tolyl)$_3$, DMPP and P(2,4,6-Me$_3$Ph)$_3$ exhibited the similar tendency with the CV data. However, XPhos and P(*o*-OMePh)$_3$ showed differences: the onset of oxidation is relatively low for XPhos (1.12 V), whereas the chemical shift value is at -12.37 ppm which represents a low donor ability. This discrepancy is because the chemical shift in ^{31}P-NMR is influenced by both steric hindrance and electron environment of the ^{31}P atoms.[46] Similarly, the small steric structure gives P(*o*-OMePh)$_3$ a lower chemical shift than what would be expected if considering only its electron donating character.

The ligands at both extremes of the electron donating ability spectrum, P(2,4,6-Me$_3$Ph)$_3$ and P(OPh)$_3$, exhibit low overall conversion to polymer (Figure 7a and 7f), which is due to unstable palladium centres. As a consequence, they fail to produce polymers of useful molecular weights and are therefore not discussed further. Increasing the steric structure of the ligand by adding an extra methyl group (e.g. in DMPP) results in a reduction of the BT conversion (Figure 7b), which is probably due to the steric demand of BT. However, increasing both the steric bulk and the electron donating properties of the ligands (such as in the cases of XPhos) leads to a much more balanced conversion of BT and BnDT yielding a statistical polymer. Decreasing the steric bulk of the ligand whilst increasing its donor ability (such as in the case of P(*o*-OMePh)$_3$) results in a slightly reduced rate for both monomers. The more electron rich palladium centre undergoes oxidative addition from the electron rich BnDT less readily and also BT experiences a reduced rate of conversion, possibly due to the extra steric clashing resulting from the rotation of the longer methoxy arm of the ligand, despite it having a lower reported cone angle.

Each of the polymers exhibits a similar molecular weight (determined by high temperature GPC), Table 2. There is little variance in the monomer composition of each polymer as determined by NMR, suggesting that any observed discrepancy

in the optoelectronic or morphological properties could be a result of the differing sequences alone.

The optoelectronic properties of the four polymers were investigated by UV-Vis spectroscopy and CV. UV-Vis spectra for each polymer film are shown in Figure 8. Each polymer film exhibits a vibronic shoulder in the region of 650-700 nm indicating a large degree of aggregation and π-stacking. The vibronic shoulder is most pronounced in the XPhos system (Figure 8a) which is the "most random" of the four polymers. In addition, this system exhibits a broader absorption profile extending into the shorter wavelengths which may be the result of the increased number of effective chromophores introduced by the more statistical distribution of donor BnDT and acceptor BT units along the back bone. Intermolecular charge transfer (ICT) peaks are seen in all four polymers in the region of 500-650 nm. The ICT states are more defined in polymers with a less statistical nature such as those synthesised using the DMPP and the Pd:P(*o*-tolyl)$_3$ systems (Figure 8b and 8d respectively).

Even in dilute solutions of chlorobenzene each polymer still displays a shoulder characteristic of aggregation, this being most noticeable with the DMPP system. Its tendency to form the "blockiest" polymers, results in BnDT-rich regions along the backbone which lead to efficient π-stacking and aggregation and thus cause a higher ordered microstructure in thin films. As each solution is heated from 25 °C to 90 °C, each polymer exhibits a blue shift due to the removal of aggregates.

The HOMO level of each polymer was estimated from the onset to oxidation potential (E_{HOMO}) as measured by CV *vs*. a ferrocene standard; the energy of the LUMO was then calculated by adding the optical energy gap, E_g, as $E_{LUMO} = E_{HOMO} + E_g^{opt}$.[44, 45] The four polymers exhibit similar values of E_g in the 1.77-1.78 eV range. The HOMO levels of the more block-like copolymers, however, are lower lying by approximately 0.1 eV, which is favourable for a greater V_{oc}.[46] Shoulders at lower potentials observed in the CV of PTBnDT-*stat*-PTBT synthesised with XPhos, P(*o*-OMePh)$_3$ and P(*o*-tolyl)$_3$ (green, blue and dark yellow traces in Figure S17, respectively) can be indicative of more crystalline domains which are more easily oxidised.[51]

Conclusions

This study has demonstrated that the catalyst used plays a key role in achieving polymeric materials with functional properties by a Stille polycondensation. We have shown that, in this instance, the Stille coupling yields polymers with a gradient/block structure arising from differences in monomer reactivity. This has been visualised by the use of STM. An ABA block type polymer is formed in one pot arising solely from the difference in monomer reactivity without the requirement for complicated monomer feeds. We have also demonstrated the significance of the choice of catalyst on the polymer formed and the resulting physical and optoelectronic properties. Whilst most catalysts systems are optimised to achieve functional molecular weights and high yields, this work has demonstrated that the effect of catalyst on monomer sequence in ternary Stille polycondensation reactions should also be considered carefully when designing functional materials for BHJ-OPV devices. We have presented simple kinetic experiments, which can be used to infer backbone sequencing of many conjugated monomers, given that one has a suitable method for quantifying monomer conversion.

Acknowledgments

We thank Merck (Chilworth UK) for funding studentships (SSL and YC) and Dr D Lester and the University of Warwick Polymer Characterization RTP for help and access to equipment. The University of Warwick is gratefully acknowledged for pump-priming funds to acquire the ESD equipment used in this work.

References

1. S. Zhang, Y. Qin, J. Zhu and J. Hou, *Advanced Materials*, 2018, **30**, 1800868.
2. N. Espinosa, M. Hosel, D. Angmo and F. C. Krebs, *Energy & Environmental Science*, 2012, **5**, 5117-5132.
3. K. Knapp and T. Jester, *Solar Energy*, 2001, **71**, 165-172.
4. C. J. Brabec, *Solar Energy Materials and Solar Cells*, 2004, **83**, 273-292.
5. H. Sirringhaus, *Advanced Materials*, 2014, **26**, 1319-1335.
6. S. Berny, N. Blouin, A. Distler, H. J. Egelhaaf, M. Krompiec, A. Lohr, O. R. Lozman, G. E. Morse, L. Nanson, A. Pron, T. Sauermann, N. Seidler, S. Tierney, P. Tiwana, M. Wagner and H. Wilson, *Advanced Science*, 2016, **3**.
7. H. Zhou, L. Yang and W. You, *Macromolecules*, 2012, **45**, 607-632.
8. Y. W. Su, Y. C. Lin and K. H. Wei, *J. Mater. Chem. A*, 2017, **5**, 24051-24075.
9. J. Q. Zhang, L. Y. Zhu and Z. X. Wei, *Small Methods*, 2017, **1**, 14.
10. S. Antohe, S. Iftimie, L. Hrostea, V. A. Antohe and M. Girtan, *Thin Solid Films*, 2017, **642**, 219-231.
11. Y. Huang, F. Liu, X. Guo, W. Zhang, Y. Gu, J. Zhang, C. C. Han, T. P. Russell and J. Hou, *Advanced Energy Materials*, 2013, **3**, 930-937.
12. P. M. Beaujuge and J. M. J. Frechet, *Journal of the American Chemical Society*, 2011, **133**, 20009-20029.
13. Z. B. Henson, K. Mullen and G. C. Bazan, *Nature Chemistry*, 2012, **4**, 699-704.
14. H. F. Yao, L. Ye, H. Zhang, S. S. Li, S. Q. Zhang and J. H. Hou, *Chemical Reviews*, 2016, **116**, 7397-7457.
15. Y. F. Li, *Accounts of Chemical Research*, 2012, **45**, 723-733.
16. A. Cetin, C. Istanbulluoglu, S. O. Hacioglu, S. C. Cevher, L. Toppare and A. Cirpan, *Journal of Polymer Science Part a-Polymer Chemistry*, 2017, **55**, 3705-3715.
17. S. W. Kim, J. Choi, T. T. T. Bui, C. Lee, C. Cho, K. Na, J. Jung, C. E. Song, B. Ma, J. Y. Lee, W. S. Shin and B. J. Kim, *Advanced Functional Materials*, 2017, **27**.
18. J. B. Howard and B. C. Thompson, *Macromolecular Chemistry and Physics*, 2017, **218**.
19. L. Liu, L. Zhang, M. Li, Y. Guo, J. Song and H. Wang, *Dyes and Pigments*, 2016, **130**, 63-69.
20. T. E. Kang, J. Choi, H. H. Cho, S. C. Yoon and B. J. Kim, *Macromolecules*, 2016, **49**, 2096-2105.

21. Q. Su, J. Tong, J. Li, P. Zhang, C. Yang, C. Zhang, F. Wang, D. Chen and Y. Xia, *Polymer Journal*, 2015, **47**, 803-809.
22. X. C. Wang, K. Wang and M. F. Wang, *Polymer Chemistry*, 2015, **6**, 1846-1855.
23. K. H. Hendriks, G. H. L. Heintges, M. M. Wienk and R. A. J. Janssen, *J. Mater. Chem. A*, 2014, **2**, 17899-17905.
24. C. Menelaou, S. Tierney, N. Blouin, W. Mitchell, P. Tiwana, I. McKerracher, C. Jagadish, M. Carrasco and L. M. Herz, *Journal of Physical Chemistry C*, 2014, **118**, 17351-17361.
25. L. Fang, Y. Zhou, Y. X. Yao, Y. Diao, W. Y. Lee, A. L. Appleton, R. Allen, J. Reinspach, S. C. B. Mannsfeld and Z. A. Bao, *Chemistry of Materials*, 2013, **25**, 4874-4880.
26. C. H. Duan, K. Gao, J. J. van Franeker, F. Liu, M. M. Wienk and R. A. J. Janssen, *Journal of the American Chemical Society*, 2016, **138**, 10782-10785.
27. W. A. Braunecker, S. D. Oosterhout, Z. R. Owczarczyk, N. Kopidakis, E. L. Ratcliff, D. S. Ginley and D. C. Olson, *Acs Macro Letters*, 2014, **3**, 622-627.
28. S. Zhang, N. E. Bauer, I. Y. Kanal, W. You, G. R. Hutchison and T. Y. Meyer, *Macromolecules*, 2017, **50**, 151-161.
29. J. Gao, W. Wang, S. Zhang, S. Xiao, C. Zhan, M. Yang, X. Lu and W. You, *J. Mater. Chem. A*, 2018, **6**, 179-188.
30. Q. Q. Zhang, M. A. Kelly, N. Bauer and W. You, *Accounts of Chemical Research*, 2017, **50**, 2401-2409.
31. W. T. Li, L. Q. Yang, J. R. Tumbleston, H. Ade and W. You, *Abstracts of Papers of the American Chemical Society*, 2014, **247**.
32. Z. Ding, J. Kettle, M. Horie, S. W. Chang, G. C. Smith, A. I. Shames and E. A. Katz, *J. Mater. Chem. A*, 2016, **4**, 7274-7280.
33. J.-H. Kim, A. Gadisa, C. Schaefer, H. Yao, B. R. Gautam, N. Balar, M. Ghasemi, I. Constantinou, F. So, B. T. O'Connor, K. Gundogdu, J. Hou and H. Ade, *J. Mater. Chem. A*, 2017, **5**, 13176-13188.
34. H. Zhou, L. Yang, A. C. Stuart, S. C. Price, S. Liu and W. You, *Angewandte Chemie-International Edition*, 2011, **50**, 2995-2998.
35. S. C. Price, A. C. Stuart, L. Yang, H. Zhou and W. You, *Journal of the American Chemical Society*, 2011, **133**, 4625-4631.
36. L. Huo and J. Hou, *Polymer Chemistry*, 2011, **2**, 2453-2461.
37. K. Zhang, R. Tkachov, K. Ditte, N. Kiriy, A. Kiriy and B. Vot, *Macromolecular Rapid Communications*, 2020, **41**.
38. S. Tierney, M. Heeney and I. McCulloch, *Synthetic Metals*, 2005, **148**, 195-198.
39. H. Bronstein, Z. Y. Chen, R. S. Ashraf, W. M. Zhang, J. P. Du, J. R. Durrant, P. S. Tuladhar, K. Song, S. E. Watkins, Y. Geerts, M. M. Wienk, R. A. J. Janssen, T. Anthopoulos, H. Sirringhaus, M. Heeney and I. McCulloch, *Journal of the American Chemical Society*, 2011, **133**, 3272-3275.
40. Z. L. Niemeyer, A. Milo, D. P. Hickey and M. S. Sigman, *Nature Chemistry*, 2016, **8**, 611-618.
41. D. J. Darensbourg, J. R. Andreatta, S. M. Stranahan and J. H. Reibenspies, *Organometallics*, 2007, **26**, 6832-6838.
42. K. Billingsley and S. L. Buchwald, *Journal of the American Chemical Society*, 2007, **129**, 3358-3366.
43. C. Cordovilla, C. Bartolome, J. M. Martinez-Ilarduya and P. Espinet, *Acs Catalysis*, 2015, **5**, 3040-3053.
44. L. Leonat, S. Beatrice Gabriela and I. V. Braîzoi, *Cyclic voltammetry for energy levels estimation of organic materials*, 2013.
45. J. L. Bredas, D. Beljonne, V. Coropceanu and J. Cornil, *Chemical Reviews*, 2004, **104**, 4971-5003.
46. C. J. Brabec, A. Cravino, D. Meissner, N. S. Sariciftci, T. Fromherz, M. T. Rispens, L. Sanchez and J. C. Hummelen, *Advanced Functional Materials*, 2001, **11**, 374-380.